A Molecular Dynamics Study of Aggregation Phenomena in Aqueous *n*-Propanol

Alfred B. Roney and Brian Space*

Department of Chemistry, University of South Florida, Tampa, Florida 33620-5250

Edward W. Castner

Department of Chemistry and Chemical Biology, Rutgers University, Piscataway, New Jersey 08854

Raeanne L. Napoleon and Preston B. Moore

Department of Chemistry and Biochemistry, University of the Sciences in Philadelphia, Philadelphia, Pennsylvania 19104

Received: December 18, 2003; In Final Form: March 1, 2004

Low-frequency Raman studies of various concentrations of aqueous *n*-propanol at room temperature indicate that both water and *n*-propanol form single-component aggregates in solution. Small-angle X-ray scattering (SAXS) and small-angle neutron scattering (SANS) studies also provide evidence of this tendency toward aggregation. Molecular dynamics simulations of 16% aqueous *n*-propanol, a concentration for which maximum segregation of *n*-propanol and water is observed, have been carried out in an attempt to elucidate the structure of these aggregates. Kirkwood−Buff integrals calculated from the radial distribution functions of the components show excellent agreement with experimentally derived values. Analysis of the atomic coordinates from the simulations reveal that approximately 50% of the *n*-propanol molecules are members of homogeneous hydrogen-bonded chains of up to 16 members in length, the majority of which are dimers. The $g(r)$ data also indicate that a strong hydrophobic association exists between the hydrocarbon tails. This hydrophobic association is independent of hydrogen-bonding state, and results in the formation of an approximately 10-member micelle structure centered around the *n*-propanol chains. Water is excluded from the regions occupied by the *n*-propanol micelles. The water structure is largely unaffected except for a small amount of disruption at the interface between the bulk solvent and the *n*-propanol clusters, and the formation of small water clusters at the interface with the bulklike solvent that interact with hydroxyl groups at the ends of the propanol chains.

1. Introduction

Aqueous solutions of aliphatic alcohols find many uses, from cleaning products and chromatography solvents to beverages and food additives. While much is known about the macroscopic chemical behavior of these solutions, the solvation structure is poorly understood for many aqueous alcohols. Multiple studies indicate that alcohol molecules aggregate in aqueous solution, but studies of the *n*-propanol aggregation indicated by Raman spectra,[1] small-angle X-ray scattering (SAXS),[2−3] small-angle neutron scattering (SANS),[4] and thermodynamic data[3,5,6] do not provide an atomistically detailed description of the microscopically heterogeneous solutions.

The existence of hydrogen-bonded chains of solute molecules has been suggested by experiments on many aliphatic alcohols.[5,7] Significant hydrophobic interactions for alcohols possessing large hydrocarbon functionalities were also indicated.[1,2,7] While many studies confirm that some sort of clustering does occur in *n*-propanol, only the hydration structures of single molecules and dilute solutions of *n*-propanol have been reported.[8] The present molecular dynamics (MD) study investigates the structure of *n*-propanol aggregates in aqueous solutions. A description of the methods that are employed is provided in Section 2. Table 1 presents the nomenclature used throughout the paper to describe the molecular structure of aqueous *n*-propanol derived from MD simulation.

TABLE 1: Nomenclature. Atom Definitions and Cluster State Prefixes Used in This Paper

Atom Symbol Definitions

symbol	definition
CA	α-carbon of *n*-propanol
CM	methyl carbon of *n*-propanol
OH	hydroxyl oxygen of *n*-propanol
HO	hydroxyl hydrogen of *n*-propanol
OW	oxygen of water

Prefix Definitions

prefix	*n*-propanol	H_2O
c	member of chain	member of bulk ($N_{cluster} \geq 10$)
u	nonchain	nonbulk

2. Background and Methodology

2.1. Raman Spectroscopy. Suggestive evidence of aggregation is present in a low-frequency Raman spectroscopy study of alcohol/water solutions.[1] The intensities of the absorption bands attributed to intermolecular O−H···O stretching between hydrogen-bonded alcohols were observed to vary in a piecewise-linear fashion with alcohol mole fraction. Additionally, the intensity of the O−H···O stretching band for water−water

* Author to whom correspondence should be addressed. E-mail: space@cas.usf.edu.

10.1021/jp037922j CCC: $27.50
Published on Web 04/22/2004

hydrogen bonds varied linearly with the water mole fraction. This linear relationship permits the Raman spectra for aqueous solutions of methanol, ethanol, *n*-propanol, 2-propanol, and *tert*-butyl alcohol to be represented as simple linear combinations of the pure components' spectra between 0 and 300 cm^{-1} according to the formula

$$R(\bar{\nu}, \chi) = aR(\bar{\nu}, 0) + bR(\bar{\nu}, 1) \quad (1)$$

where $R(\bar{\nu}, \chi)$ is the Raman signal at $\bar{\nu}$ wavenumbers, χ is the mole fraction of alcohol, and a and b are coefficients. Since both bands of interest are intermolecular stretching modes, their linear variance with concentration indicates that the hydrogen-bond structure of both components is largely unaffected in solution. This implies that despite the fact that *n*-propanol and water are infinitely miscible, the solution is far from homogeneous and suggests that both *n*-propanol and water form aggregates that mimic, at least spectroscopically, the structure of the respective pure components.

For *n*-propanol, the intermolecular O−H···O stretching band of interest is located at 69 cm^{-1}. The coefficients a and b, while regionally linear, exhibit inflection points at 20 and 50% mole-fraction of *n*-propanol, in agreement with the respective minimum and maximum of the heat of mixing for *n*-propanol. These inflection points coincide with a suspected transition from *n*-propanol clusters in water solvent at $\chi_p < 10\%$, to separate clusters of *n*-propanol and water at $20\% \leq \chi_p \leq 60\%$, and finally to water clusters in the *n*-propanol solvent at $\chi_p > 60\%$.[1] These distinctions, however, are only qualitative observations without a molecularly detailed explanation. Nonetheless, formation of different solvation structures with concentration is strongly suggested by these observations, and MD is an ideal method to identify the structures involved.

2.2. Aggregate Structures. Much of the existing work on aqueous solutions of low-molecular-weight aliphatic alcohols indicates that the hydroxyl groups from the alcohol molecules form hydrogen-bonded chains, with the alkyl tails extending into the solvent. In this structure, each hydroxyl oxygen donates and accepts one hydrogen from another hydroxyl group, for a total of two hydrogen bonds per molecule of alcohol.[5] X-ray diffraction and mass spectrometry studies[7] indicate that for methanol these chains take two forms, cis- and trans-, based upon the orientation of the alkyl groups. The number of molecules comprising these chains is directly proportional to the concentration of methanol, and the O−O spacing along the chains decreases ~4% as the mole fraction varies from $\chi_m = 0\%$ to $\chi_m = 100\%$. Ethanol, 2-propanol, and *tert*-butyl alcohol also exhibit similar behavior.

Several differences in the aggregation behavior of *n*-propanol compared to other alcohols have been noted. One significant difference is the temperature dependence of the Debye correlation length, an indication of the correlation distance of density fluctuations in a solution.[9] While the correlation length of *tert*-butyl alcohol exhibits a temperature dependence, the correlation length of *n*-propanol is independent of temperature. The temperature dependence for *tert*-butyl alcohol is attributed to the "melting" of an ice-like cage structure surrounding the *tert*-butyl group with increasing temperature; therefore, the lack of temperature dependence for *n*-propanol suggests that no similar hydration structure exists around the *n*-propyl groups.[10,2] Additionally, no clathrate−hydrate crystal structure of *n*-propanol has been observed, despite the existence of these structures for 2-propanol and *tert*-butyl alcohol. This indicates a significant difference in the hydration structure of *n*-propanol when compared to these similar molecules, and suggests that the alkyl tails of *n*-propanol disrupt the water structure enough to prevent the formation of a hydrogen-bonded water network surrounding the hydrophobic functionalities. It also suggests that these functional groups may be excluded from the water structure by solute aggregation.

Animations of the system were produced from the MD simulations and rendered in order to obtain a qualitative visual idea of the aggregation phenomena. Snapshots of individual configurations were taken highlighting different molecular solvation phenomena including, for example, sorting species by their hydrogen-bonding environment. As an example, Figure 1(a−c) presents a snapshot of a typical *n*-propanol−water MD simulation with all species 1(b) and the water 1(a) and *n*-propanol 1(c) removed. Details are presented below.

2.2.1. Hydrogen-Bonded Neighbor Search. Since hydrogen bonding is the primary method of aggregation indicated by spectroscopic data, a search for hydrogen bonds was performed on each atomic configuration using criteria from the literature.[11] The criteria were implemented as follows. A search for oxygen atom pairs possessing an interatomic radius of 2.5−3.2 Å was performed. Among oxygen pairs identified as possessing the correct separation, the intermolecular hydrogen−oxygen distance (r_{OH}) was calculated for each hydrogen that was molecularly bonded to a member of the candidate O−O pair. If r_{OH} fell between 1.5 and 2.2 Å, the prospective hydrogen-bond angle formed by the candidate O−H···O triad (θ_{OHO}) was calculated. If θ_{OHO} fell between 130° and 180°, the respective molecules were considered to be hydrogen-bonded. From the identification of hydrogen-bonded pairs, coordination numbers were calculated and individual aggregates of molecules were identified. Detailed histograms of chain and cluster sizes were also calculated for various species and subspecies described below.

2.2.2. Nth-Nearest-Neighbor Histograms. A set of histograms were generated for various pairs of atoms i and j by calculating all radial distances r_{ij} for each molecule of species i and saving them in an array. This array was then sorted into ascending order, and the seven smallest distances were used to increment the corresponding bin of seven separate histograms. The histograms were normalized by dividing the bin counts by the number of species i present, and averaged by dividing each bin by the number of configurations analyzed. This resulted in a separate histogram of the radial distance to each of the first seven neighbors of a given species; this analysis is useful in discerning the variation in solvation structure of a given species. For example, while many water molecules are tetrahedrally bonded, some are shown below to have between 0 and 5 hydrogen-bonded neighbors, and up to 7 neighbors at hydrogen-bonding distance. The nearest-neighbor distributions for OW−OW, CA−CA, CM−CM, CA−OW, CM−OW, OH−OH, and OH−OW were calculated.

2.3. Radial Distribution Functions. To make connection with experiment and to further understand the solution structure, various radial distribution functions, $g_{ij}(r)$ were calculated. The radial distribution function is formally defined for isotropic systems by[12]

$$g_{ij}(r) = \frac{\rho_j(r_{ij})}{\rho_{id}(r_{ij})} = \frac{\rho_j(r_{ij})}{\langle \rho_j \rangle} \quad (2)$$

where $\rho_j(r_{ij})$ is the average number density of species j in a spherical shell of radius r_{ij} centered at species i, and $\rho_{id}(r_{ij})$ is the density of an ideal gas at the same number density $\langle \rho_j \rangle$ as molecule j. The radial distribution function is easily calculated from the coordinate output of a molecular dynamics simulation

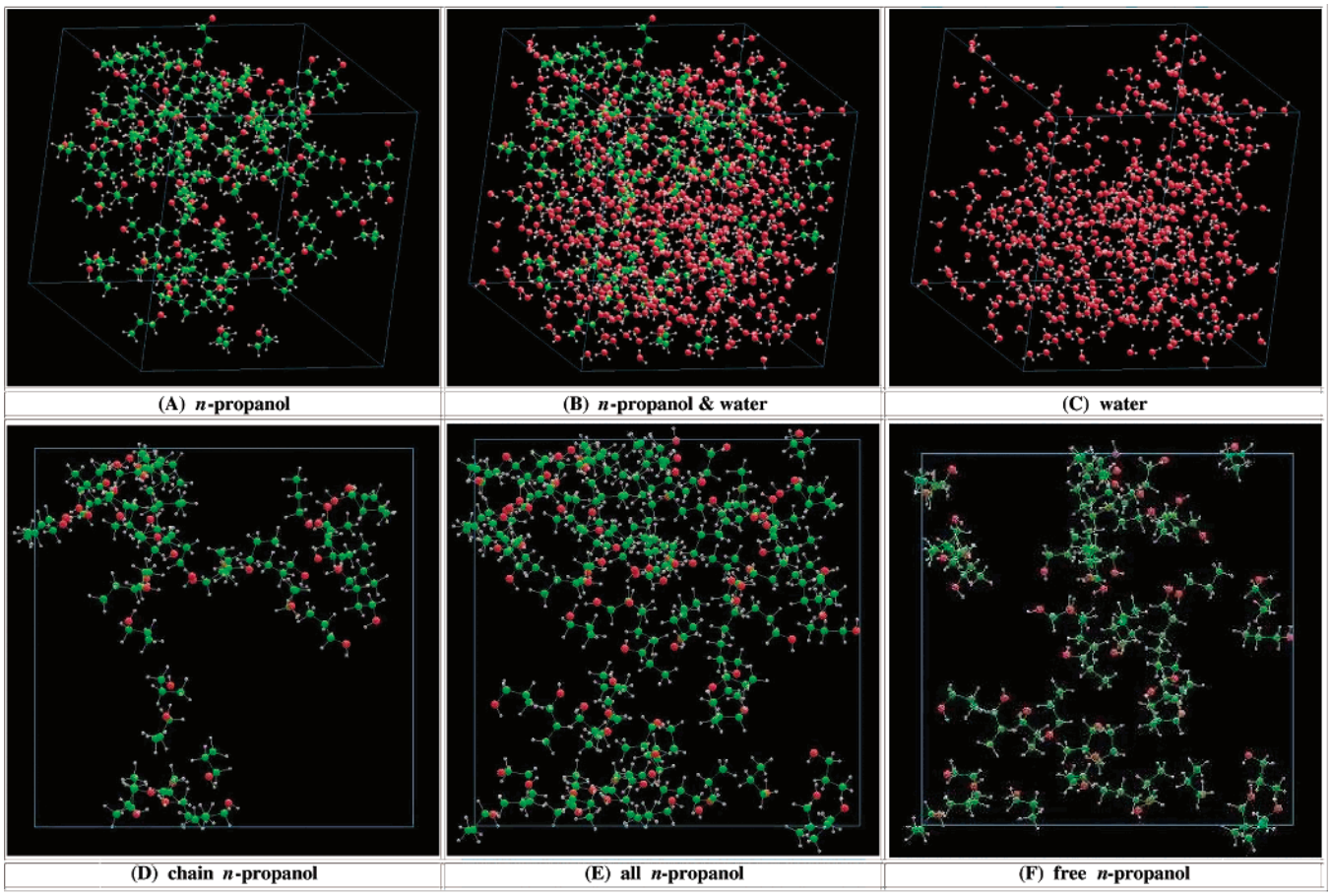

Figure 1. Snapshots of two representative configurations from the molecular dynamics simulation. Water and *n*-propanol do not intermingle appreciably, in accordance with experimental evidence. Additionally, hydrogen-bonded chains of *n*-propanol molecules aggregate with other chains and with free *n*-propanol through a hydrophobic association of their alkyl groups.

by creating a histogram of the radial distances r_{ij}, calculating the average density of species *j* within the spherical shell defined by the bin location and dimensions, and dividing the resulting density by the ensemble average density of *j* to give $g_{ij}(r)$ at the location of the center of the bin.

The species represented by *i* and *j* can be either the center of mass of a molecule, or any atom of interest on a molecule. In this paper they are also chosen to represent the center of mass or a specific atom from the same type of molecule in a specific aggregation state, such as molecules that are members of a hydrogen-bonded chain (as defined by a chosen set of criteria defined below). These functions provide a good description of the short-range order present in liquids.[13] They also allow the estimation of single-component aggregate sizes by integrating over the first-neighbor peak:

$$\langle N_i \rangle = 1 + 4\pi\langle\rho_i\rangle \int_0^{r_{\min}} g_{ii}(r) r^2 \, dr \qquad (3)$$

where $\langle\rho_i\rangle$ is the average number density of species *i*. By choosing $r_{\min}$ as the location of the first minimum in $g_{ii}(r)$, $\langle N_i \rangle$ becomes the number of molecules comprising an aggregate.

Molecular radial distribution functions were generated for solute−solute ($g_{pp}(r)$), solute−solvent ($g_{pw}(r)$), and solvent−solvent ($g_{ww}(r)$) using the center of mass of the molecules as their location. These results were compared to $g_{ij}(r)$ data calculated using the α-carbon coordinates of *n*-propanol (CA) and the oxygen coordinates of water (OW) as the molecular coordinates due to the proximity of these atoms to the center of mass. Additionally, *functional* radial distribution functions were calculated, including $g_{OH-OH}(r)$, $g_{OH-HO}(r)$, and $g_{OH-OW}(r)$.

As described in Section 4.2, both solute and solvent can be sorted into groups according to their hydrogen-bonding state, resulting in the creation of four species: *chain n*-propanol, *free n*-propanol, *bulk* water, and *nonbulk* water. Chain *n*-propanol molecules are defined as *n*-propanol molecules that are hydrogen-bonded to other *n*-propanol molecules. Free *n*-propanol molecules are not hydrogen-bonded to any other *n*-propanol molecules. Bulk water is defined as water clusters consisting of 10 or more members, as determined from the coordination data. All remaining water molecules are considered to be a separate species from the bulk. *Functional* radial distribution functions were calculated for these four species in order to decompose both the *molecular* and *functional* radial distribution functions and illuminate the various intermolecular interactions responsible for the observed aggregation.

2.4. Kirkwood−Buff Integrals. Kirkwood−Buff integrals,[14] G_{ij}, are derived from integrals of $g_{ij}(r)$ and can be considered to be a measure of the *average* excess or deficit of species *j* around species *i*. This makes G_{ij} an excellent measure of the degree of aggregation. They are formally defined by

$$G_{ij} = \int_0^{\infty} [g_{ij}(r) - 1] 4\pi r^2 \, dr \qquad (4)$$

Kirkwood−Buff integrals were computed from the radial distribution functions using a trapezoid-rule based integration routine. G_{pp}, G_{pw}, G_{ww}, G_{CA-CA}, G_{CA-OW}, G_{OW-OW}, G_{OH-OH}, and G_{OH-OW} were calculated and compared to experiment. While there is no extant direct experimental measurement of $g_{ij}(r)$ for aqueous alcohols, G_{ij} can be experimentally measured by a variety of methods. Since they are easily calculated from the

TABLE 2: Harmonic Oscillator Potential Parameters. Harmonic Oscillator Potential Parameters Used for the Molecular Dynamics Simulations ($V_{HO}(r) = {}^1/_2 k_f(r - r_{eq})^2$)

atom pair	k_f(K/Å^2)	r_{eq}(Å^2)
	n-propanol	
C−C	311903	1.526
C−H	342088	1.09
C−O	321965	1.41
O−H	556395	0.96
	water	
O−H	556395	0.9572
H−H	556395	1.5136

TABLE 3: Torsion Potential Parameters. Torsion Potential Parameters for *n*-Propanol Used for the Molecular Dynamics Simulations, in Kelvins (K) ($V_{torsion}(\phi) = {}^1/_2 \sum_k p_k \cos^k(\phi)$)

atom sequence	p_0	p_1	p_2	p_3
X_1−C−O−X_2	41.9225	−125.767	0.00	167.69
X_1−C−C−X_2	39.1277	−117.383	0.00	156.511

TABLE 4: Lennard-Jones Potential Parameters. Lennard-Jones Potential Parameters Used to Model Intermolecular and One-Four Intramolecular Interactions ($V_{LJ}(r) = 4\epsilon[(\sigma/r)^{12} - (\sigma/r)^6]$)

atom	σ (Å)	ϵ (K)
C	3.39967	55.0359
$H_{aliphatic}$	2.47135	7.8982
$O_{propanol}$	3.06647	105.846
O_{water}	3.15075	76.4666

$g_{ij}(r)$ data obtained from MD simulations, they are used in this paper as a convenient comparison to experiment and serve to validate the MD models used in the present investigations.

3. Molecular Dynamics Methods

3.1. Computational Details. The MD production runs produced trajectories by solving dynamical equations of motion using a modified form of the velocity-Verlet algorithm that takes advantage of multiple time-step integration.[15] Modified OPLS parameters were used.[16,17] All molecules were flexible, and harmonic stretching and bending interactions were used. The harmonic potential parameters are presented in Table 2. For *n*-propanol, torsions were represented by a power series using the coefficients presented in Table 3. Additionally, one-four intramolecular interactions were represented by Lennard-Jones potentials presented in Table 4.

Intermolecular interactions were modeled by Lennard-Jones 6-12 potentials and electrostatic interactions. The Lennard-Jones parameters used to model the intermolecular potentials were identical to the parameters used to model intramolecular one-four interactions. The electrostatic potential surfaces were represented by partial-charges located on specified atoms of each molecule. Long-range electrostatic interactions were calculated using Ewald sums.[18] For *n*-propanol, the hydroxyl oxygen was assigned a charge of −0.728 *e*, the hydroxyl hydrogen was assigned a charge of +0.431 *e*, and the α-carbon was assigned a charge of +0.297 *e*. The remaining atoms bore no charges. This charge distribution produced a dipole moment of 2.36 *D*. While substantially larger than the gas-phase dipole moment (1.68 *D*), this value mimics the increase in the dipole moment observed for polar molecules in the condensed phase, and is proportionally similar to the increase in dipole moment for liquid-phase water.[19] For water, the oxygen atom was assigned a charge of −0.82 *e* and the hydrogens were assigned charges of +0.41 *e*. These model parameters produced aqueous *n*-propanol solution densities in good agreement with experimental measurements over a broad range of concentrations.[20]

Simulations of 16% mole fraction *n*-propanol in water were performed using a 2523 atom system. This system consisted of 91 *n*-propanol molecules and 477 SPCE water molecules, with cubic periodic boundary conditions. A Linux Beowulf cluster composed of 1.8 GHz AMD Athlon nodes performed the computations, using the MPI version of a code developed at the Center for Molecular Modeling at the University of Pennsylvania, which uses reversible integration and extended system techniques.[15,21] The processing load was distributed over two nodes, which resulted in a processing rate of 0.90 s per time step with a 1.0 fs time step.

The simulation was carried out in three phases. In the first phase, an initial set of atomic coordinates which evenly distributed the *n*-propanol and water molecules on a simple cubic lattice was assigned random velocities sampled from a Gaussian distribution, and the velocities were scaled so that the initial temperature was 293 K. The system was allowed to equilibrate in the isothermal−isobaric (NPT) ensemble using extended Lagrangian techniques.[15] Multiple time-scale integration was used, with the long-range intermolecular forces calculated every 1.0 fs, forces due to torsions calculated every 0.5 fs, and other intramolecular forces calculated every 0.125 fs. Quantities of interest, such as the volume, temperature, pressure, and total (extended system) and component energies, were monitored every 0.01 ps. The external pressure was set to 1.0 atm and the barostat frequency was chosen as 1.0 ps^{-1}.[15,22]

The second phase began once a stable volume had been achieved through a 100 ps simulation. Volume data were collected for 2.0 ns. From this the average volume was calculated, and the periodic boundaries were adjusted from their instantaneous values to the calculated values. This converted the system to an NVT ensemble with an overall density of 0.91 g/cm^3, which is in reasonable agreement with the accepted value of 0.9311 g/cm^3.[19] Each atom in the system was then assigned a new random velocity sampled from a Gaussian distribution. The velocities were initially scaled to give a temperature of 4.0 K, and the system was allowed to equilibrate for 1.0 ps at this temperature in order to resolve any bad contacts resulting from the sudden change of the periodic boundary length without disrupting the aggregate structure. This second equilibration was necessary since the atomic coordinates were not scaled to fit the new periodic boundaries. A further NVT simulation of 9.0 ps at 293 K then ensured that the system dynamics were stable.

In the final production phase atomic coordinates were collected for subsequent analysis. First, 100 sets of 10.0 ps each were collected and used to calculate $g_{ij}(r)$. Using time-dependent plots of $g_{ij}(r)$ from the equilibrating system, it was determined that the radial distribution functions had converged to stable values after 200 ps, suggesting that equilibrium had been achieved. To analyze the structure of the solute clusters, a 2 ns simulation was performed to generate the atomic configurations analyzed using the various methods described above.

For comparison, control systems of pure *n*-propanol and water were simulated using identical potential parameters. For *n*-propanol, a 256-molecule simulation was used equilibrated in a manner identical to the mixed system. This gave a density of 0.86 g/cm^3, a value within 6.4% of the accepted value of 0.8034 g/cm^3.[19] For water, a 512-molecule system was prepared using the same method, resulting in a density of 0.95 g/cm^3. This value is within 5.2% of the experimental density of pure water (0.9982 g/cm^3).[19] Both systems were used to generate 2 ns of configurations in the NVT ensemble. These sets of atomic coordinates

TABLE 5: Kirkwood−Buff Integral Results. G_{ij} Values Calculated from the $g_{ij}(r)$ Data Presented in Figures 4 and 5 Compared to Results from Small-Angle Neutron Scattering (SANS)[4] and Small-Angle X-ray Scattering (SAXS)[2] Experiments (Note that experimental agreement deteriorates when the site of hydrogen bonding, i.e., the oxygen atom, is not used as the location of the molecule.)

molecule pair		G_{ij}		
i	*j*	MD	SANS	SAXS
n-propanol	*n*-propanol		1109	1270
OH	OH	1044		
CA	CA	1395		
n-propanol	H_2O		−1129	−1210
OH	OW	−1176		
CA	OW	−1342		
H_2O	H_2O		818	960
OW	OW	1032		

were then analyzed using the same methods as the simulated solution to generate comparison data.

4. Results and Discussion

4.1. Model Validation. Kirkwood−Buff Integral values compared with experimental data are presented as Table 5. While the correct way to calculate the integrals is to calculate the distance and angular dependent distribution function and integrate over the angle variables, this is very computationally demanding and the present approximation was sufficient for comparison purposes. Table 5 demonstrates the good agreement that is obtained when the integrals are performed with the hydroxyl oxygen or α-carbon of the propanol. Using the hydroxyl oxygen, the resulting values differ by only 6% and 4%, respectively, providing strong evidence that the system model is reasonable. The overall agreement of G_{ij} values from the MD simulation with experimental results confirms that the model system is a good representation of the aggregation phenomena observed by experiment.

From visual inspection of the system animation it can be observed that *n*-propanol formed exclusive aggregates in agreement with conclusions from the Raman and scattering studies.[1−4] As shown in Figure 1(a), not displaying the water molecules revealed large open spaces occupied by bulk water, and not displaying the *n*-propanol molecules in Figure 1(c) revealed that the aggregates were largely anhydrous. Figures 1(d−f) show a snapshot of subsets of *n*-propanol molecules grouped according to chain membership as defined above. It is apparent that the chains themselves self-aggregate in addition to hydrophobic association with the free *n*-propanol.

4.2. Hydrogen-Bond Coordination Results. Despite the evidence of component structure preservation in the Raman spectra, the coordination data presented in Table 6 indicate that the hydrogen-bonding structures of both *n*-propanol and water

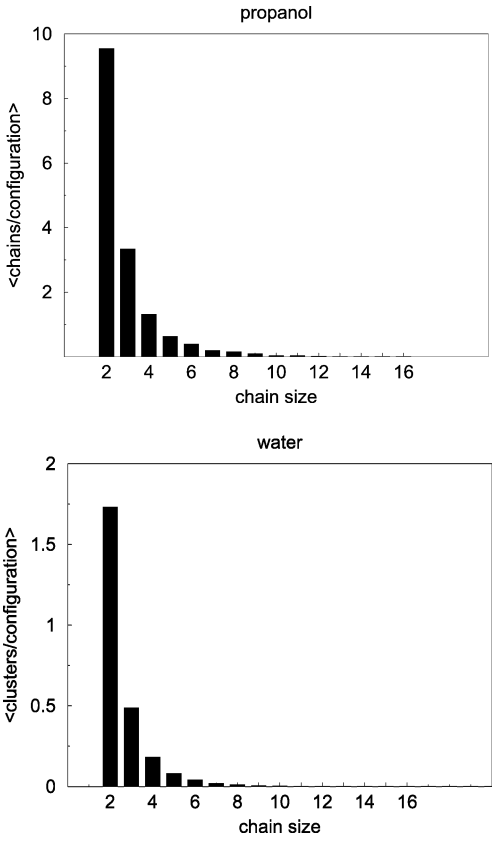

Figure 2. Histogram of the average number of *n*-propanol chains or water clusters of a given size (number of molecules) observed in an average configuration.

are signifigantly affected upon mixing. While only slightly more than 1% of the alcohol molecules do not form hydrogen bonds with other alcohol molecules in the neat simulations, more than half of the alcohol molecules are "free" in the mixture. Furthermore, the occurrence of triple-coordinated molecules in the neat simulation is nearly seven times the occurrence of triple-coordination in the presence of water. The structure of pure water is similarly disrupted in the presence of *n*-propanol. Almost five times the number of "free" water molecules were found in the solution simulation when compared to the control system, and an overall reduction in hydrogen bonding was observed compared to the pure water simulation.

The hydrogen-bonding data reveal much about the types of aggregation phenomena present. On average, approximately 46 *n*-propanol molecules out of 91 (51%) do not form hydrogen bonds with other *n*-propanol, approximately 32 molecules are singly coordinated with other *n*-propanol, and approximately 12 *n*-propanol are doubly coordinated. On average, one triple-

TABLE 6: Hydrogen-Bond Coordination Numbers. Percentage of the Central Molecule Having the Specified Number of Hydrogen Bonds with the Coordinating Molecule[a]

molecule pair		coordination number					
central	coordinated	0	1	2	3	4	5
n-propanol	*n*-propanol	51.26%	35.06%	13.14%	0.55%	0.00%	0.00%
n-propanol	water	16.67%	34.60%	35.75%	12.79%	0.19%	0.00%
water	*n*-propanol	76.83%	19.12%	3.58%	0.45%	0.02%	0.00%
water	water	1.90%	11.75%	30.06%	36.17%	19.09%	1.03%
pure *n*-propanol		1.07%	13.50%	81.76%	3.66%	0.001%	0.00%
pure water		0.41%	5.65%	23.58%	40.39%	28.17%	1.78%

[a] For example, 12.79% of the *n*-propanol molecules are hydrogen-bonded to three water molecules, while 0.45% of the water molecules are hydrogen-bonded to three *n*-propanol molecules. Included for comparison in the bottom two rows are the self-coordination data for simulated systems of *n*-propanol and water, respectively. Insignificant occurences of coordination numbers greater than 5 are not included in this table.

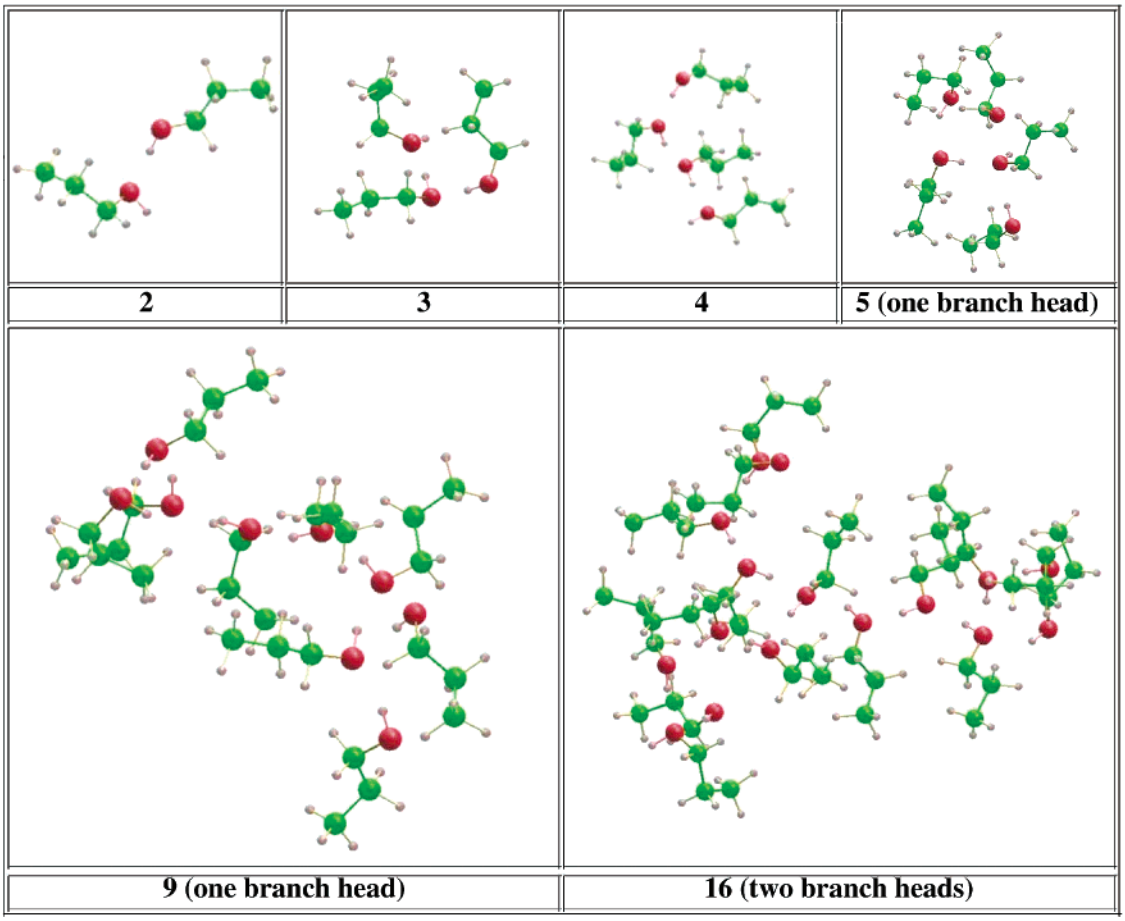

Figure 3. Snapshots of hydrogen-bonded chains of *n*-propanol representing the various chain sizes present. A "branch head" is an *n*-propanol molecule that accepts two hydrogen bonds from *n*-propanol and donates one to a third *n*-propanol, resulting in a "fork" in the chain. Note that the alkyl tails form a large hydrophobic volume that shields the chain backbone from exposure to the solvent.

coordinated *n*-propanol molecule was observed in half of the configurations, resulting in a branched chain. Since the singly coordinated *n*-propanol molecules terminate the chains, ignoring the branched chains indicates that an average configuration contains 16 chains. If it is assumed that no chains larger than three members in size exist, the coordination data imply that at least four chains (25%) are dimers. If we assume that only one chain with more than two members exists, then a maximum of 94% of the chains can be dimers. The coordination histogram of *n*-propanol in Figure 2 confirms that in fact more than half of the chain aggregates are dimers, and that chains of up to four *n*-propanol appear in every atomic configuration sampled. Chains of up to sixteen members were observed, albeit infrequently. Snapshots of several chains taken from various sets of atomic coordinates are included as Figure 3. In these chains, the alkyl tails of *n*-propanol turn away from the chain backbone of O−H···O hydrogen bonds, presumably due to steric effects. In this manner, the larger chains create a structure similar to a highly branched hydrocarbon molecule, which results in a large hydrophobic surface area for the chain. This structure also shields the hydrogen bonds from interaction with the bulk solvent, which may be responsible for the linear independence of the O−H stretching bands for *n*-propanol and water.[1]

The coordination data presented in Table 6 also suggest that the aggregate structure is micellar in nature. Despite the existence of large single-component regions in the liquid, substantial hydrogen bonding between *n*-propanol and water was observed. Since only ~17% of the *n*-propanol molecules were not hydrogen-bonded to water while slightly less than half of all *n*-propanol molecules were members of chains, it can be deduced that water forms hydrogen bonds to the O−H···O backbone of the chains. If we assert that alcohols participate in a maximum of two hydrogen bonds, then one can imply that these hydrogen bonds occur only at the terminal hydroxyl groups of the chains.[5] This long-held theory is contradicted, however, by the observance of a substantial percentage of *n*-propanol molecules possessing 3 hydrogen bonds to water. Due to the water-exclusion observed in the system visualizations, it can be assumed for this system that the chain−water interactions occur primarily at the ends of the chains. Further evidence of this hypothesis is presented in Section 4.4.

The aggregate structure disrupts the structure of bulk water at the interface to some degree, as determined from data presented in Table 6. Here we find that, on average, 1.03% of water molecules are coordinated with five other waters, 1.90% of water molecules are free of any hydrogen bonds to other water molecules, and most water molecules are forming two-four hydrogen bonds, consistent with a disrupted tetrahedral network reminiscent of neat liquid water. An interesting occurrence is the existence of a significant number of water molecules (3.58%) hydrogen-bonded to two *n*-propanol molecules, suggesting the existence of composite chains. Given the number of *n*-propanol molecules doubly coordinated with water, at least one *n*-propanol−water chain exists. There are possibly up to 15 (*n*-propanol)$_2$(H_2O) trimers in an average configuration, with the remaining doubly coordinated waters forming bridges between an *n*-propanol chain and a free *n*-propanol or chain. This is a possible mechanism to explain the proposed shift to

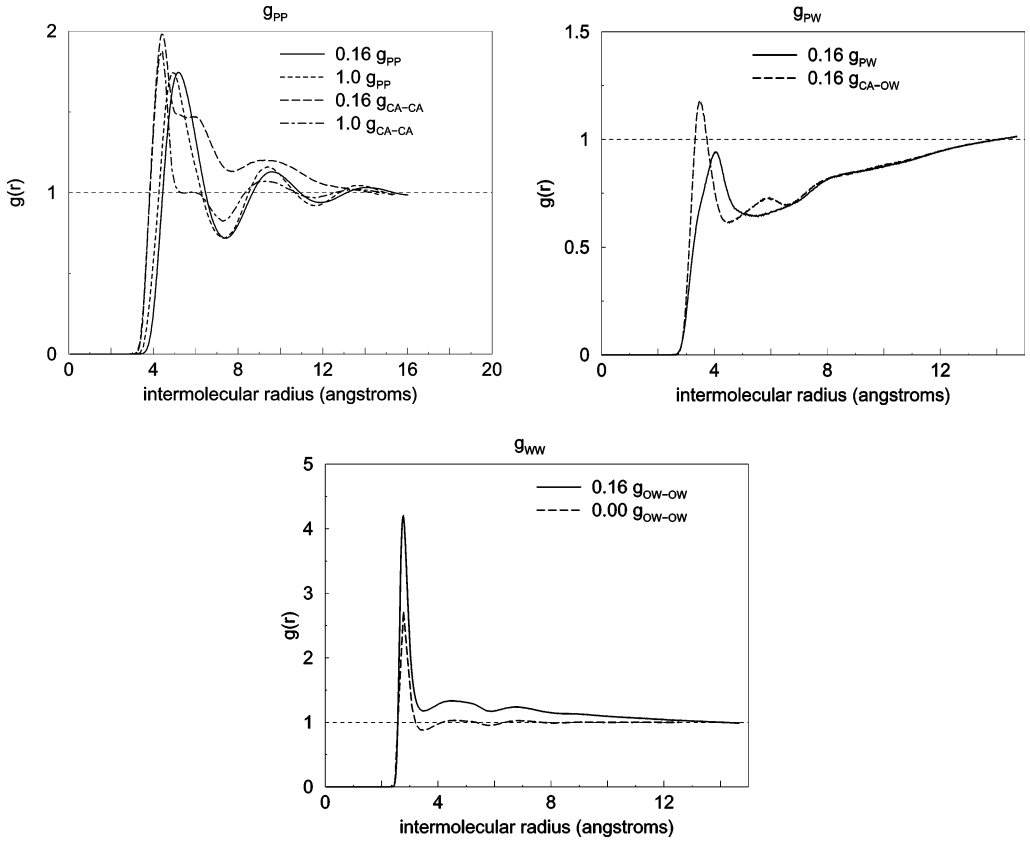

Figure 4. Plots of $g_{ij}(r)$ vs distance, r, for *n*-propanol−*n*-propanol ($g_{pp}(r)$), *n*-propanol−water ($g_{pw}(r)$), and water−water ($g_{ww}(r)$). Lines labeled with the subscripts "p" and "w" used the center of mass of the respective molecules as the location of the molecule. All other lines used the subscripted atom as the location of the molecule. Concentrations are given as mole fraction of *n*-propanol. Note that for 16% *n*-propanol, $g_{pp}(r)$ is nearly identical to $g_{pp}(r)$ for 100% *n*-propanol.

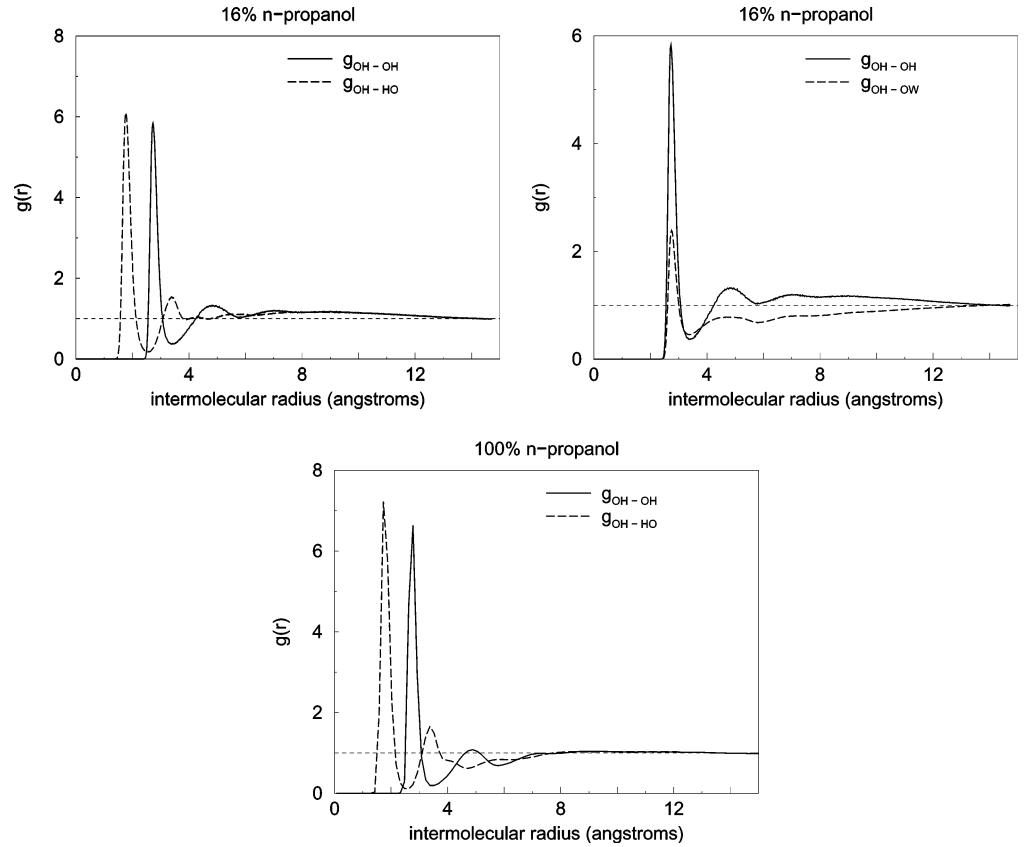

Figure 5. Comparison of $g_{OH-OH}(r)$ with $g_{OH-OW}(r)$ and $g_{OH-HO}(r)$. The alternating peaks of $g_{OH-OH}(r)$ and $g_{OH-HO}(r)$ for the 16% *n*-propanol solution are indicative of hydrogen-bonded chains. This alternating structure is clearly observable in the neat *n*-propanol data. Also note the similarity of the peak structures of $g_{OH-OH}(r)$ and $g_{OH-OW}(r)$ for the 16% *n*-propanol solution.

water clusters in bulk *n*-propanol for concentrations above $\chi_p = 0.6$. The occasional observance of coordination with three or more *n*-propanol molecules corroborates this idea, which will be the subject of future research.

Figure 2 presents a histogram of the sizes of small water aggregates observed. In addition to the one large cluster of bulk water observed in every configuration (not shown), small clusters of up to 23 water molecules were observed. The majority of these small clusters are dimers, and Figure 9 demonstrates that they occur primarily at the interface between *n*-propanol aggregates and bulk water. This figure also indicates that, surprisingly, the free waters exist primarily in the regions occupied by the bulk solvent. Small clusters of 10 or more waters appear so infrequently that they were considered bulk water for the cluster-state-dependent $g(r)$ data discussed in Section 4.4.

4.3. Molecular Distributions. The molecular and functional $g(r)$ plots in Figures 4 and 5 provide further characterization of the types and extent of aggregation phenomena. In the *n*-propanol−*n*-propanol case, $g_{pp}(r)$ from Figure 4 is nearly identical to $g_{pp}(r)$ for neat *n*-propanol. This is strong evidence that the structure of neat *n*-propanol is preserved in aqueous solution. The first peak of $g_{pp}(r)$ for the aqueous solution, when integrated using eq 3, indicates that the average *n*-propanol cluster is comprised of ~10 members, much larger than any commonly observed chain in the simulation. This discrepancy can be attributed to hydrophobic association.

Despite the proximity of CA to the center of mass, $g_{CA-CA}(r)$ differs significantly from $g_{pp}(r)$, revealing that the first peak in $g_{pp}(r)$ actually is the average of at least two types of first-neighbor interactions for the aqueous solution. The sharp first peak at 4.5 Å can be thought of as a chain signature, and the broad shoulder from 5 to 6.5 Å can be attributed to the hydrophobic association of alkyl tails from neighboring *n*-propanol molecules. This structural feature of $g_{CA-CA}(r)$ also exists in the data for the pure *n*-propanol system, although the magnitudes of the individual features are modulated. The similar intensities of the first peak result from the higher extent of hydrogen bonding in the neat system. The elevated hydrophobic shoulder on the plot for the solution indicates that the alkyl tails are localized, resulting in the increased ratio of their density at this radius compared to the overall density of *n*-propanol in the solution. The similarities in the line shapes of the two systems suggest that the aggregates resemble regions of pure *n*-propanol surrounded by pure water.

Figure 5 provides evidence of both chain formation and hydrophobic aggregation of multiple chains. The location of the first-neighbor peak of $g_{OH-OH}(r)$ slightly off center between the first and second peaks of $g_{OH-HO}(r)$ is an unmistakable signature of the O−H···O atom sequence of the chains, as is the similarity in the peak spacing between $g_{OH-OH}(r)$ and $g_{OH-OW}(r)$. The existence of slight third- and fourth-neighbor peaks confirms the persistence of chains having at least five members. Identical short-range features exist in the control system data, but the absolute magnitudes of the data for the solution are slightly elevated above the controls due to aggregation. One important difference in the two systems is the broad rise from 6 to 14 Å in $g_{OH-OH}(r)$ for the solution. This feature results from the hydrophobic association of neighboring chains through their alkyl tails. This attribution will be discussed further in Section 4.4.

The size and spacing of the aggregates can be discerned by comparing $g_{pw}(r)$ with $g_{pp}(r)$. The large trough from 4.5 to 7.65 Å results from water exclusion inside the *n*-propanol aggregates,

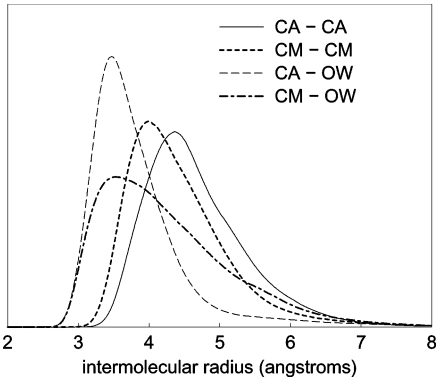

Figure 6. Distributions of the radial distance to the first neighbor for CA−CA, CM−CM, CA−OW, and CM−OW. Note the near unimodality of the distributions.

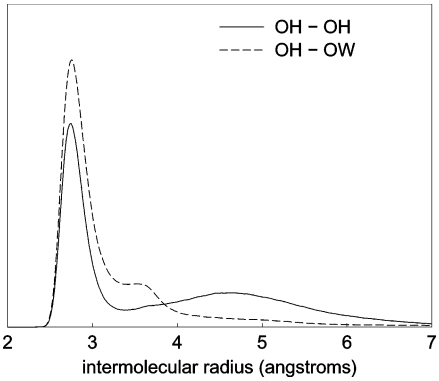

Figure 7. Distributions of the radial distance to the first neighbor for OH−OH and OH−OW. Note the bimodality of the distributions.

and also indicates that the aggregates exhibit an average radius of 7.65 Å. Its coincidence with the first peak of $g_{pp}(r)$ shows that the first peak in $g_{pp}(r)$ is indeed representative of aggregation, and that the clusters are spaced an average of 9.6 Å apart.

Further evidence of two types of interactions between *n*-propanol can be observed by comparing $g_{pw}(r)$ with $g_{CA-OW}(r)$. The first-neighbor peak of $g_{pw}(r)$ exhibits bimodality, with a slight peak at 3.5 Å growing from the side of a larger peak at 4.2 Å. The first peak coincides with the first-neighbor peak of $g_{CA-OW}(r)$, indicating that two mechanisms of interaction with water exist for *n*-propanol. Furthermore, the mechanism that results in a closer association to the center of mass does not occur very often, suggesting that one of the species defined by this interaction is shielded from bulk water. Furthermore, while $g_{CA-OW}(r)$ shows evidence of exposure to bulk water in its regularly spaced humps and troughs, the center-of-mass based $g_{pw}(r)$ lacks this pattern. This is compelling evidence for the existence of a micelle structure.

The data presented in Figures 6 and 7 justify the division of *n*-propanol into two species on the basis of the hydrogen-bonding state. Figure 6 shows the first-neighbor distance distributions for the hydrophobic section of the *n*-propanol molecule, and their unimodality reveals that their mechanism of association is independent of chain state. Furthermore, the broadness of the CA−CA and CM−CM peaks corresponds to the amorphous nature of these nonpolar interactions. The coincidence of the maximum of CA−OW and CM−OW at 3.5 Å indicates that their interaction with the bulk is parallel to the interface, suggesting a cylindrical micelle structure centered around the chain backbone. This is corroborated by the long tail of the CM−OW curve, which indicates that a significant portion of the methyl groups are buried inside the aggregates.

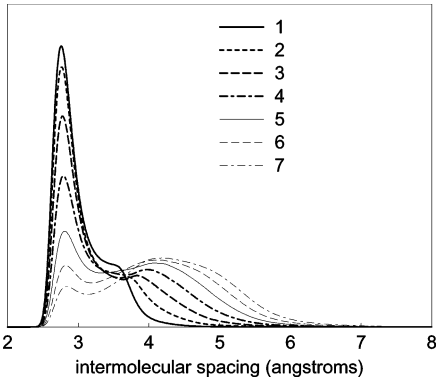

Figure 8. Distributions of the radial distance between water oxygens for the first seven neighbors. Note that up to seven water molecules are found in the first coordination sphere, despite the fact that no more than 5 hydrogen bonds were observed for a single water molecule in the 16% *n*-propanol solution. Also note that the plateau on the first-neighbor distribution is similar to the first-neighbor distribution for OH−OW.

Also worthy of mention is the lack of a shoulder from 5 to 6.5 Å on the CA−CA curve, which suggests that the α-carbons aggregate independently of hydrogen bonding, despite their proximity to the hydroxyl group.

Since the chain structure for *n*-propanol places the α-carbons in such close proximity, it is surprising that two peaks representing the chain and free species were not observed in the CA−CA first-neighbor histogram. This supports the idea that hydrophobic aggregation is independent of hydrogen bonding, and also provides further evidence of composite chains. The histogram of OH−OH distances from Figure 7 indicates that the hydroxyl groups of *n*-propanol molecules are separated by 2.75 Å in the chains and by 4.6 Å for free *n*-propanol. The spacing of the free *n*-propanol from this graph coincides with the second-neighbor peak from $g_{OH-OH}(r)$ from Figure 5. When considered in light of the coordination data and the lack of a second peak in the first-neighbor distribution for CA−CA, this indicates that the contribution of composite *n*-propanol−water chains is significant. These composite chains are interpreted as comprising the outer layer of a two-species micelle, with the hydroxyl groups from the composite chains forming hydrogen bonds with the bulk water, and suspending the hydrophobic chain structures in the solvent through the interaction of their propyl groups with those of the chain members.

Significant water structure disruption can be determined by the existence of up to seven water neighbors at hydrogen-bond distance for water, as demonstrated by coincident peaks at 2.75 Å in all the distributions presented in Figure 8. The first-neighbor distribution also indicates that water can be divided into two species on the basis of cluster size. While most free water exists either in the bulk solvent or at the solvent−aggregate interface, as observed in Figure 9, the hump in the first-neighbor distribution for OW−OW indicates that occasionally a water molecule is pulled away from the interface by an *n*-propanol molecule. Cluster-state-dependent $g_{OH-OW}(r)$ data confirm that interfacial extraction does occur for both single water molecules as well as for small clusters, which is discussed further in Section 4.4.

4.4. Cluster-State-Dependent Radial Distribution Functions. From the analysis of data presented and discussed above, it was determined that *n*-propanol formed a chain-centered micelle structure with a layer of disrupted water at the interface. Radial distribution functions were generated which treated chain and free *n*-propanol as separate species, and used the small water

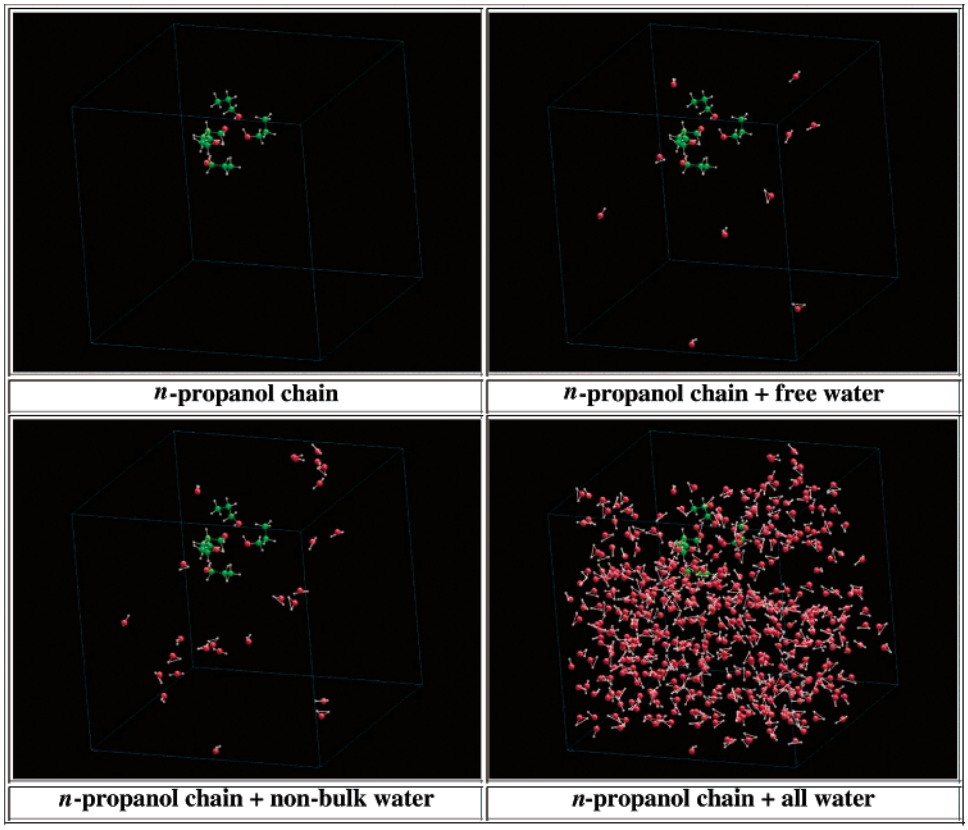

Figure 9. Snapshots of a representative configuration from the molecular dynamics simulation are shown that display the nature of solvation for a single aqueous *n*-propanol cluster with the surrounding *n*-propanol molecules hidden for visualization. The solvating water is characterized as free (not hydrogen-bonded to other water molecules), clustered, and bulklike. Note that the clustered and free water molecules form a curved interface between the bulk water region and the region occupied by the *n*-propanol aggregates.

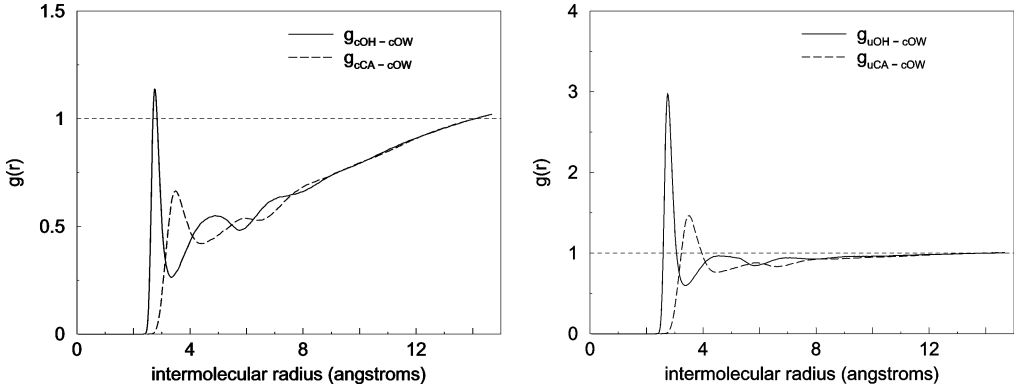

Figure 10. Cluster-state-dependent $g(r)$ plots showing the interactions of the hydrophilic end of *n*-propanol with bulk water. Note that $g_{uOH-cOW}(r)$ is quite similar in structure to $g_{OW-OW}(r)$ for neat water from Figure 4.

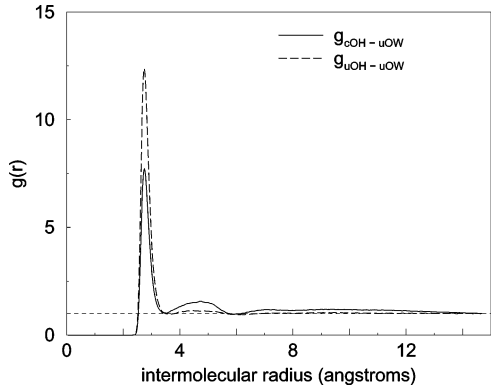

Figure 11. Cluster-state-dependent $g_{OH-uOW}(r)$. Note that only $g_{cOH-uOW}(r)$ has a significant second-neighbor peak for nonbulk waters, indicating that the chain ends are more likely to extract small clusters from the solvent−micelle interface.

clusters as an approximate way to divide water into bulk solvent and disrupted water in order to probe the water structure disruption at the *n*-propanol aggregate−bulk water interface. In Figure 10, the first-neighbor peak intensity ratios for both $g_{uOH-cOW}(r)/g_{cOH-cOW}(r)$ and $g_{uCA-cOW}(r)/g_{cCA-cOW}(r)$ are ∼3:1. This reveals that the free *n*-propanol molecules are three times more likely than chain *n*-propanol to be hydrogen-bonded to bulk water. This strengthens the idea that free *n*-propanol molecules form a surrounding layer that shields the chains from exposure to bulk water.

The broadening of the second peak in $g_{uOH-cOW}(r)$ may indicate that water structure disruption does occur at the aggregate interface, but that this disruption does not usually result in the complete extraction of a small solvent cluster. Despite the tendency of the *n*-propanol chains to be surrounded by free *n*-propanol, the signature of the water structure in $g_{cOH-cOW}(r)$ indicates that they are exposed to the bulk solvent to a significant degree, and that their exposure does not result in the same type of structure disruption that is observed for the free *n*-propanol. This also agrees with the idea of an oblong spherical micelle structure, since it indicates that the chain ends are not always shielded from the bulk.

Figure 11 provides evidence that the extraction of small water clusters occurs primarily at the interface between the ends of the chains and the bulk solvent. The existence of a second-neighbor peak in $g_{cOH-uOW}(r)$ that is hardly discernible in $g_{uOH-uOW}(r)$ indicates that the free *n*-propanol is less likely to pull a small cluster into the aggregate region. Free *n*-propanol is more likely to disrupt the water structure, however, as indicated by the lack of broadening of the second-neighbor peak in $g_{cOH-cOW}(r)$.

The tendency of the free *n*-propanol to turn alkyl groups away from the bulk solvent and toward other alkyl groups is described by Figure 12. The ∼3:2 ratio of intensities for the slight first-neighbor peaks of $g_{uCM-cOW}(r)/ g_{cCM-cOW}(r)$ supports the idea of a micelle structure since it indicates that free *n*-propanol molecules are exposed to a higher number of water molecules. Both $g_{cCM-cOW}(r)$ and $g_{uCM-cOW}(r)$ show a marked deficit in the density of water in close coordination with the hydrophobic portion of *n*-propanol. They also lack the 2.75 Å peak spacing signature associated with exposure to the solvent. The lack of a sharp first-neighbor peak for both $g_{cCM-cOW}(r)$ and $g_{uCM-cOW}(r)$ indicates that the small amount of close association of the methyl group and water occurs without a well-defined structure. Both functions also exhibit a region of depressed intensity extending to 7.5 Å which coicides with the water-exclusion trough observed in $g_{pw}(r)$.

The independence of the hydrophobic association in cluster formation can also be seen in Figure 12. An overall similarity in the structure of CM−CM interactions, as indicated by coincident peaks at 4 Å, 5.25 Å, and 8−9 Å, as well as a similar minimum at 7 Å, indicates that the alkyl tail interaction results in the same type of hydrophobic association regardless of chain state. The overall elevation of intensity of $g_{cCM-cCM}(r)$ can be attributed to the large hydrophobic surface area presented by the chains, which results in a greater tendency to aggregate, but its similarity in structure to $g_{cCM-uCM}(r)$ and $g_{uCM-uCM}(r)$ asserts that the hydrophobic interaction mechanism is unaffected by hydrogen bonding at the hydroxyl group.

The chain−chain hydrophobic aggregation interpreted from $g_{OH-OH}(r)$ is confirmed by $g_{cOH-cOH}(r)$ from Figure 13. Distinct neighbor peaks can be observed out to the fourth neighbor, indicating five-member chains. The third- and fourth-neighbor peaks lie on top of a broad region of increased intensity from 6 to 13.5 Å which coincides with the second peak in $g_{pp}(r)$. This chain−chain aggregation results from the hydrophobic association of the alkyl tails, which are turned out and away from the hydrogen-bond backbone. In this manner, the chains aggregate with themselves as if each chain were a highly branched hydrocarbon, since the hydrophilic groups are only exposed to the bulk solvent at the ends of the chains, and are possibly further shielded from bulk water by micellar *n*-propanol molecules and water−*n*-propanol composite chains attached to the chain terminus.

Further evidence of the existence of the composite chains can be found in Figure 13. The regular peak structure of $g_{OH-OH}(r)$ appears in all three $g(r)$ plots. Since the chain structure is defined by hydrogen bonding, $g_{cOH-cOH}(r)$ exhibits a very strong peak at 2.75 Å, and the lack of intensity for

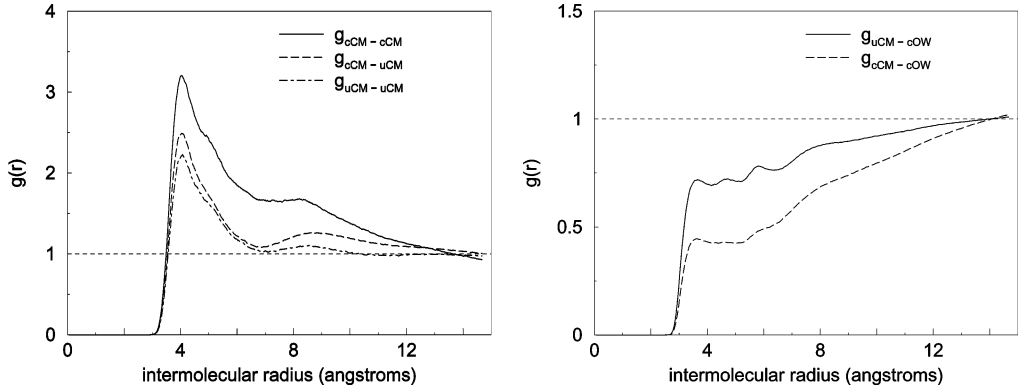

Figure 12. Cluster-state-dependent $g(r)$ plots showing the interactions of the hydrophobic end of *n*-propanol. The similarities in the line shapes indicate that the alkyl tail interactions are independent of the hydrogen-bonding status of *n*-propanol.

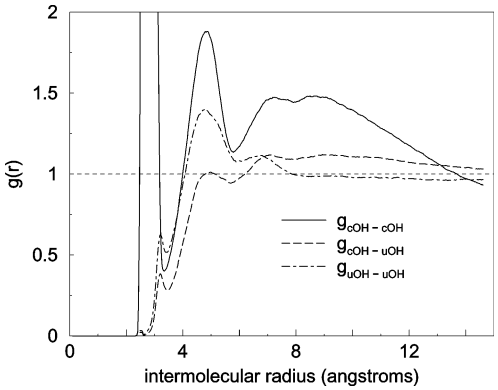

Figure 13. Cluster-state-dependent $g_{OH-OH}(r)$. Note that the first-neighbor peaks for interactions involving free *n*-propanol coincide with the second-neighbor peak for the *n*-propanol chains, neglecting the remnants of chain formation observed between 0 and 3.5 Å. This is strong evidence for the existence of composite chains of the form (*n*-propanol)−$(H_2O)_x$−(*n*-propanol).

$g_{cOH-uOH}(r)$ and $g_{uOH-uOH}(r)$ in the region between 2.5 and 3.25 Å indicates that unless *n*-propanol molecules are hydrogen-bonded together, their hydroxyl groups do not associate closely. Free *n*-propanol instead tends to associate with both free and chain *n*-propanol at a spacing of 5 Å, which coincides with the second-neighbor peaks of $g_{OH-OH}(r)$, $g_{OH-OW}(r)$, $g_{OW-OW}(r)$, and $g_{cOH-cOH}(r)$. This indicates that both species participate in composite chains, where *n*-propanol molecules are displaced from the chain backbone and substituted by a water molecule. The existence of first- and second-neighbor peaks at 5 Å and 7 Å, repectively, in $g_{uOH-uOH}(r)$ indicates that both (*n*-propanol)−(H_2O)−(*n*-propanol) and (*n*-propanol)−$(H_2O)_2$−(*n*-propanol) structures form, with the single-water structure preferred. Similar structures also join chains and composite chains, as determined by the similar peak structures of $g_{cOH-uOH}(r)$. Furthermore, these chain−composite chain structures participate in chain−chain hydrophobic aggregation, as the general rise in $g_{cOH-uOH}(r)$ from 6.5 to 14.75 Å demonstrates.

Up to this point, little has been said about the micelle structure other than the observation that the methyl groups tend to bury themselves in an oblong spherical aggregate structure. The micelles appear to be largely amorphous, with no well-defined structures observed other than the pure and composite chains. Specifically, $g_{uCM-cCM}(r)$ from Figure 12 exhibits the same first-neighbor peak location as both $g_{cCM-cCM}(r)$ and $g_{uCM-uCM}(r)$, which rules out the existence of micelle structures where the free *n*-propanol molecules insert into the spaces between the alternating pendant alkyl groups of the chains. The chains and composite chains tend to be excluded from the water structure much like a hydrocarbon, and are suspended in the solution by the micellar *n*-propanol molecules. These micellar *n*-propanol molecules form an interface between the aggregates and the solvent by donating hydrogen bonds to the water structure, and turning their alkyl groups toward the aliphatic shell surrounding the chain backbones.

5. Conclusion and Future Direction

The analysis of the molecular dynamics indicates that at 16% mole fraction, *n*-propanol forms an amorphous micelle centered around a hydrogen-bonded chain structure resembling the pure *n*-propanol structure. These structures consist of both pure *n*-propanol chains, as well as chains that include water molecules in the hydrogen-bond backbone. These chains turn their pendant alkyl groups out and away from the backbone, and the resulting structure resembles a highly branched aliphatic hydrocarbon with hydrophilic sites at the ends of the chains. The nonpolar aliphatic regions of the clusters then aggregate together in a manner similar to branched-chain hydrocarbons in water, and are suspended in the polar solvent by *n*-propanol molecules which turn their alkyl tails inward toward the chains and form hydrogen bonds with the solvent, disrupting the water structure out to the second hydration sphere, as determined by peak broadening in $g_{OH-OW}(r)$. This structure is best described as small "droplets" of neat *n*-propanol emulsified by the "free" *n*-propanol molecules. A simplified schematic representation of the aggregate structure is included as Figure 14.

The current method of sorting water into bulk solvent and interfacial water needs refinement. Since the present method uses only the hydrogen-bonding data to sort the water molecules, a highly disrupted cluster of water needs only one hydrogen bond to the bulk solvent to be considered a part of the bulk. A more comprehensive method of water structure analysis should be implemented. One possibility is the use of order parameters such as those used by Fidler and Rodger,[8] which take into account the near tetrahedral bonding angles of water.

The ability of the chain terminal hydroxyl groups to extract small clusters of water from the bulk solvent is significant in that it provides a mechanism for the transition from separate clusters of *n*-propanol and water at $\chi_p \leq 60\%$ to water clusters in *n*-propanol solvent at $\chi_p > 60\%$. It is suspected that as the concentration of *n*-propanol is increased, both the number and size of the small water clusters will increase, and these clusters will be cut off from the each other by surrounding *n*-propanol at the highest concentrations. Additionally, as the mole fraction

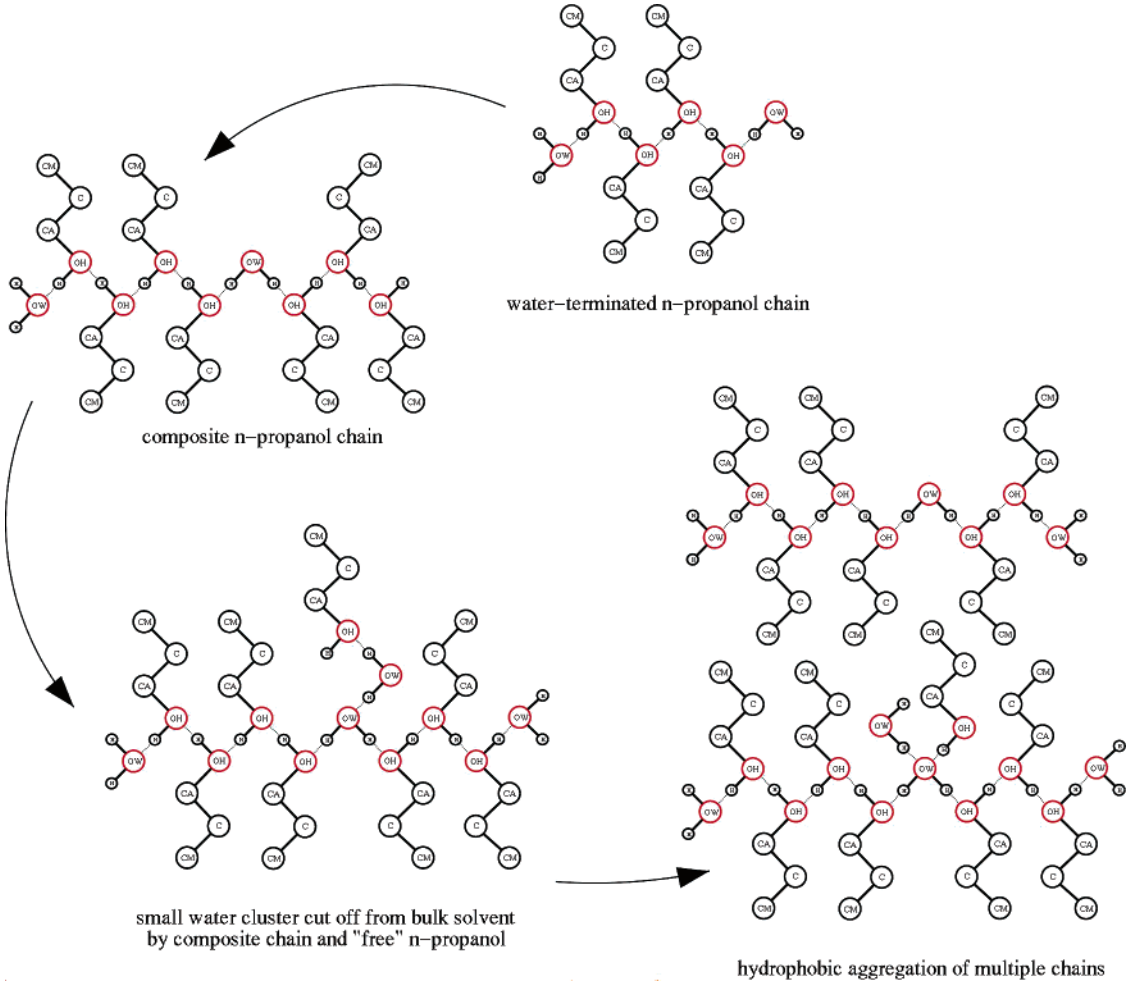

Figure 14. Simplified two-dimensional diagram of the types of structures observed in the solution. Oxygen atoms are highlighted in red. Molecular bonds are indicated by solid black lines, and hydrogen bonds are represented by dotted lines. The alkyl hydrogens are not shown. Starting from the top and proceeding counterclockwise, the hydrogen-bonded chains which dominate the structure of pure *n*-propanol are shortened and terminated by hydrogen bonds to water molecules. Adjacent chains form composite chains via bridging water molecules, which can extract and isolate small water clusters from the solute−solvent interface. Due to the large hydrophobic volume created by the pendant propyl groups (see Figure 3), individual and composite chains tend to aggregate to minimize solvent exposure. The outer layers of free *n*-propanol (not shown) form micelles centered around the structures presented here.

is reduced to $\chi_p < 10\%$, the transition to *n*-propanol clusters in bulk solvent should also be observed by a reduction in the size and number of small water clusters formed. These hypotheses are being investigated in ongoing studies, and the results will be reported in future publications.

Another topic of interest is the percentage of structure disruption for both *n*-propanol and water, as investigated by Raman spectroscopy.[1] Simulations of the low-frequency Raman spectroscopy will be performed for various mole fractions of *n*-propanol, in an attempt to replicate the linear combination of spectra observed by experiment. Additionally, the structure disruption observed in this study should result in an increase in the amount of free O−H stretching signal present in the IR spectrum for water, and should produce peak components that are similar to the IR spectrum of either gas-phase or interfacial water. This is currently an active area of research, and the results will be presented in future publications.

Acknowledgment. The authors acknowledge the use of the services provided by the Research Oriented Computing Center, University of South Florida. The research at USF was supported by an NSF Grant (No. CHE-0312834) and a grant from the Petroleum Research Foundation to Brian Space.

References and Notes

(1) Yoshida, K.; Yamaguchi, T. Low-frequency Raman spectroscopy of aqueous solutions of aliphatic alcohols. *Z. Naturforsch.* **2001**, *56 a*, 529−536.

(2) Hayashi, H.; Nishikawa, K.; Iijima, T. Small-angle X-ray scattering study of fluctuations in 1-propanol−water and 2-propanol−water systems. *J. Phys. Chem.* **1990**, *94*, 8334−8338.

(3) Shulgin, I.; Ruckenstein, E. Kirkwood-Buff integrals in aqueous alcohol systems: Comparison between thermodynamic calculations and X-ray scattering experiments. *J. Phys. Chem. B* **1999**, *103*, 2496−2503.

(4) Almásy, L.; Jancsó, G.; Cser, L. Application of SANS to the determination of Kirkwood−Buff integrals in liquid mixtures. *Appl. Phys. A, 74[Suppl.]* **2002**, S1376−S1378.

(5) Franks, F.; Ives, D. J. G. The structural properties of alcohol−water mixtures. *Q. Rev. Chem. Soc.* **1966**, *20*, 1−44.

(6) Matteoli, E.; Lepori, L. Solute−solute interactions in water. ii. An analysis through the Kirkwood-Buff integrals for 14 organic solutes. *J. Chem. Phys.* **1984**, *80* (6), 2856−2863.

(7) Takamuku, T.; Yamaguchi, T.; Asato, M.; Matsumoto, M.; Nishi, N. Structure of clusters in methanol−water binary solutions studied by mass spectrometry and X-ray diffraction. *Z. Naturforsch.* **2000**, *55 a*, 513−525.

(8) Fidler, J.; Rodger, P. M. Solvation structure around aqueous alcohols. *J. Phys. Chem. B* **1999**, *103*, 7695−7703.

(9) Debye, P. Angular dissymmetry of the critical opalescence in liquid mixtures. *J. Chem. Phys.* **1959**, *31*, 680−687.

(10) Frank, H. S.; Evans, M. W. Free volume and entropy in condensed systems. iii. Entropy in binary liquid mixtures; partial molal entropy in dilute solutions; structure and thermodynamics in aqueous electrolytes. *J. Chem. Phys.* **1945**, *13*, 507−532.

(11) Jeffrey, G. A. *An Introduction to Hydrogen Bondin*g; Oxford: New York, 1997.

(12) Allen, M. P.; Tildesley, D. J. *Computer Simulation of Liquid*s; Clarendon Press: Oxford, 1989.

(13) McQuarrie, D. A. *Statistical Mechanics*; Harper and Row: New York, 1976.

(14) Kirkwood, J. G.; Buff, F. P. The statistical mechanical theory of solutions. I. *J. Chem. Phys.* **1951**, *19*, 774−777.

(15) Tuckerman, M.; Berne, B. J.; Martyna, G. J. Reversible multiple time scale molecular dynamics. *J. Chem. Phys.* **1992**, *97*, 1990.

(16) Jorgensen, W. L.; Maxwell, D. S.; Tirado-Rives, J. Development and testing of the OPLS all-atom force field on conformational energetics and properties of organic liquids. *J. Am. Chem. Soc.* **1996**, *118*, 11225−11236.

(17) Cornell, W. D.; Cieplak, P.; Bayly, C. I.; Gould, I. R.; Merz, K. M.; Ferguson, D. M.; Spellmeyer, D. C.; Fox, T.; Caldwell, J. W.; Kollman, P. A. A second generation force field for the simulation of proteins, nucleic acids, and organic molecules. *J. Am. Chem. Soc.* **1995**, *117* (19), 5179−5197.

(18) Ewald, P. Die berechnung optischer und elektrostatischer gitterpotentiale. *Ann. Phys.* **1921**, *64*, 253−287.

(19) Lide, D. R. *Handbook of Chemistry and Physics*, 84th ed.; CRC Press LLC, New York, 2003.

(20) Roney, A. B.; Space, B.; Moore, P. B.; Castner, E. W. A molecular dynamics study of the concentration dependence of aggregation phenomena in aqueous *n*-propanol. To be submitted.

(21) Moore, P. B.; Zhong, Q.; Husslein, T.; Klein, M. L. Simulation of the hiv-1 vpu transmembrane domain as a pentameric bundle. *FEBS Lett.* **1998**, *431*, 143−148.

(22) Paci, E.; Marchi, M. Constant-pressure molecular dynamics techniques applied to complex molecular systems and solvated proteins. *J. Phys. Chem.* **1996**, *100*, 4314−4322.